frontiers | Frontiers in Marine Science

TYPE Original Research
PUBLISHED 14 September 2022
DOI 10.3389/fmars.2022.984989

OPEN ACCESS

EDITED BY
Shiguo Li,
Research Center for Eco-environmental Sciences, (CAS), China

REVIEWED BY
Chuang Liu,
Hohai University, China
Jingliang Huang,
Tsinghua University, China

*CORRESPONDENCE
Qinzeng Xu
xuqinzeng@fio.org.cn;
xqz08@163.com

SPECIALTY SECTION
This article was submitted to Marine Molecular Biology and Ecology, a section of the journal Frontiers in Marine Science

RECEIVED 03 July 2022
ACCEPTED 19 August 2022
PUBLISHED 14 September 2022

CITATION
Ge M, Mo J, Ip JC-H, Li Y, Shi W, Wang Z, Zhang X and Xu Q (2022) Adaptive biomineralization in two morphotypes of Sternaspidae (Annelida) from the Northern China Seas. *Front. Mar. Sci.* 9:984989. doi: 10.3389/fmars.2022.984989

Adaptive biomineralization in two morphotypes of Sternaspidae (Annelida) from the Northern China Seas

Meiling Ge[1,2], Jing Mo[2], Jack Chi-Ho Ip[3], Yixuan Li[2,3], Wenge Shi[2], Zongling Wang[1,2], Xuelei Zhang[2] and Qinzeng Xu[2*]

[1]College of Environmental Science and Engineering, Ocean University of China, Qingdao, China, [2]Key Laboratory of Marine Eco-Environmental Science and Technology, First Institute of Oceanography, Ministry of Natural Resources, Qingdao, China, [3]Department of Biology, Hong Kong Baptist University, Kowloon, Hong Kong SAR, China

Polychaetes are segmented annelid worms that play a key role in biomineralization in modern oceans. However, little is known about the underlying processes and evolutionary mechanisms. The ventro-caudal shield of Sternaspidae is a typical phosphate biomineral in annelids. Here, we investigated two sternaspids from the northern China Seas, *Sternaspis chinensis* and *Sternaspis liui* syn. n, which evolved diverse shield characteristics as local adaptation. Genetic distances, phylogenetic analyses of nuclear markers (*18S* and *28S* genes), and mitochondrial genomes revealed that the latter is a junior synonym of the former. The integration of elemental composition and the transcriptomic analysis provided insights into phenotypic shield differences. The electron probe microanalysis showed that shields in *S. chinensis* were more biomineralized (i.e., with higher iron, phosphorus, and calcium contents) than those in *S. liui* syn. n. Transcriptomes of the body wall around shields determined 17,751 differentially expressed genes (DEGs) in two morphotypes of the synonymous species. Function enrichment analysis of DEGs showed that *S. chinensis* has an enrichment of the putative biomineralization pathways (i.e., ion transport and calmodulin binding), while *S. liui* syn. n consumed more energy and produced more proteins (i.e., oxidative phosphorylation and ribosome). DEGs allowed to identify seven shell matrix proteins expressed differentially in the two morphotypes, especially calponin, filamin, chitinase, and protease inhibitor BPTI/kunitz, which might contribute to shield evolutionary plasticity response to their living habitats. Overall, this study 1) revealed an environmental biomineralization adaptation in two polychaete morphotypes of one species by integrating shield chemical composition of shields and transcriptome analyses and 2) provided insights into the molecular mechanisms underlying polychaete biomineralization.

KEYWORDS

biomineralization, shell matrix protein, Sternaspidae, shield composition, mitochondrial genome, transcriptome

Introduction

Biomineralization is a biological process allowing living organisms to produce minerals. In invertebrates, biomineralization has been mainly studied in mollusks, corals, brachiopods, bryozoans, and echinoderms (Takeuchi et al., 2016; Malachowicz and Wenne, 2019; Clark, 2020; Murdock, 2020). However, polychaetes are also important biomineralization organisms in marine environments whose study will help in understanding biomineralization and evolutionary adaptation in invertebrates (Vinn, 2021). The tubes of serpulids, sabellids, and cirratulids are composed of calcite, aragonite, or a mixture of both (Vinn, 2021). Serpulid tubes contain soluble and insoluble organic matrices that control biomineralization (Tanur et al., 2010). Sabellids and cirratulids are characteristic of matrix-mediated biomineralization (Vinn et al., 2008; Vinn, 2021). The formation of the chitinous tube in the deep-sea siboglinid tubeworm *Paraescarpia echinospica* is also controlled by matrix proteins (Sun et al., 2021). Other polychaetes produce biominerals as parts of their bodies (e.g., chaetae, elytra, and shields) (Heffernana1, 1990; Vinn, 2021). However, little is known about their chemical composition and formation in these cases.

The ventro-caudal shields are typically phosphate biominerals in Sternaspidae (Polychaeta: Terebellida) and some Fauveliopsidae, formed by amorphous ferric phosphate hydrogel (composed of FeO, P_2O_5, CaO, MgO, BaO, and MnO) (Lowenstam, 1972; Sendall and Salazar-Vallejo, 2013). Particularly, sternaspids were considered key animals in oceanic ferric phosphate hydrogel-sinking processes (Lowenstam, 1972) due to their worldwide distribution from shallow to deep waters (Salazar-Vallejo and Buzhinskaja, 2013).

In addition, shield morphology is a diagnostic feature for the four genera of Sternaspidae (*Sternaspis* Otto, 1821, *Caulleryaspis* Sendall & Salazar-Vallejo, 2013, *Petersenaspis* Sendall & Salazar-V allejo, 2013 and *Mauretanaspis* Fiege & Barnich, 2020) and 43 valid species (Fiege and Barnich, 2020). Recently, however, *Sternaspis sendalli* and *Sternaspis monroi* proved to be genetically identical based on the mitochondrial cytochrome oxidase I (*COI*) and *16S* ribosomal RNA (*16S*) markers despite having different shield features (Drennan et al., 2019).

Sternaspids are habitually found in China seas, especially in the Bohai and Yellow Seas (Jin-Bao et al., 2006), while Wu et al., (2015) described *Sternaspis chinensis* Wu, Salazar-Vallejo & Xu, 2015 and *Sternaspis liui* Wu, Salazar-Vallejo & Xu, 2015 from the northern China Seas. *S. chinensis* has a stiff shield with easy-to-brush sediment particles attached, while *S. liui* has a slightly sclerotized and soft shield with firmly adhered sediment. Based on *COI* and *16S* and the nuclear *18S* ribosomal RNA (*18S*) and *28S* markers, we have revealed that they are genetically identical, *S. liui* (Wu et al., 2015) syn. n being a junior synonym of *S. chinensis*. This led us to question the molecular mechanisms contributing to shield evolutionary plasticity of the two morphotypes.

Therefore, this study aims at 1) further confirming *S. chinensis* and *S. liui* syn. n as two morphotypes being the same species based on sequencing their mitochondrial genomes, 2) revealing the shield chemical composition leading to the observed stiffness, and 3) elucidating the gene regulatory mechanisms underlying biomineralization.

Materials and methods

Specimen collection, morphological identification, and molecular taxonomy

Specimens of *S. chinensis* and *S. liui* syn. n (Yellow Sea) were collected using an Agassiz trawl (Figure 1, Table S1) and those of *S. sendalli* (South Shetland Islands) and *Sternaspis buzhinskajae* (Salazar-Vallejo, 2014) (Arctic Ocean) with a box corer. These two polar species were used to analyze the genetic distance and phylogeny of the two morphotypes of synonymous species (Figure 1, Table S1). All specimens were preserved in 75% ethanol for morphological examination and DNA extraction or directly frozen at −80°C for RNA extraction on board.

Shield morphological features (Figures S1–S4) were analyzed following Wu et al. (2015) using a Nikon SMZ1270 stereomicroscope and NIS-Elements 4.50 software. Species identity was further confirmed by amplifying fragments of *COI*, *16S*, *18S*, and *28S* and comparing the obtained sequences (Tables S1, S2) with those available in GenBank. The uncorrected paired *p* distances of *COI*, *16S*, *18S*, and *28S* between and within species were calculated by the Kimura 2-parameter (K2P) model implemented in MEGA v7.0.26 (Kumar et al., 2016).

Mitochondrial genome sequencing and analysis

Total genomic DNA was extracted from body walls around shields using MicroElute Genomic DNA Kit (OMEGA, USA). Genomic DNA libraries with an insert size of approximately 350 bp were constructed with NEBNext® Ultra™ DNA Library Prep Kit (Illumina, USA) and sequenced on the Illumina Hiseq 2500 sequencer (Illumina, USA) in Qingdao Insight Exbio Technology Corporation (China) to generate 150-bp paired-end reads. Raw reads were quality controlled and filtered using FastQC v0.11.9 (Andrews, 2010) and Trimmomatic v0.39 (Bolger et al., 2014), respectively, under default parameters. Clean reads were assembled using SPAdes v3.13 (Nurk et al., 2013) under default settings. The putative mitochondrial contig was identified using BLASTn against the available annelid mitogenome in the NCBI database. The mitogenome was annotated using the MITOs webserver (Bernt et al., 2013)

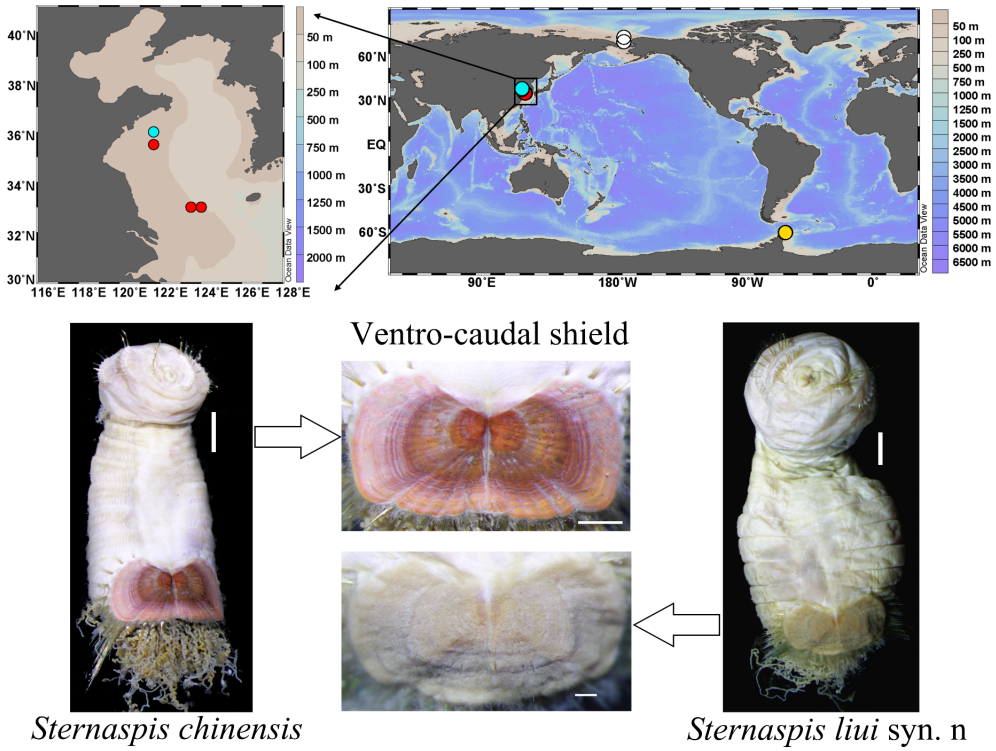

FIGURE 1
Sampling locations of sternaspid specimens used in the present study and morphological images of two sternaspids from the China Seas. Red circle, *Sternaspis chinensis*; cyan circle, *Sternaspis liui* syn. n; white circle, *Sternaspis buzhinkajae*; yellow circle, *Sternaspis sendalli*. Scale bars: *S. chinensis* body = 2 mm, shield = 1 mm; *S. liui* syn. n body = 2 mm, shield = 500 µm.

under default settings with the invertebrate mitochondrial genetic code. The gene start and stop codons were manually inspected and adjusted by MEGA v7.0.26 (Kumar et al., 2016). All assembled mitochondrial genomes were deposited in GenBank (Table S3).

Thirteen protein-coding genes (PCGs) and two rRNA genes of 27 polychaetes with complete mitogenomes, covering all families of Sedentaria, as well as those of *Chloeia pocicola* and *Cryptonome barbada* (outgroups) deposited in GenBank were used for the phylogenetic analysis (Table S3). Maximum likelihood (ML) analysis was analyzed by IQ-TREE v. 1.6.8 (Nguyen et al., 2015) with 1,000 bootstrap replicates (Supplementary Material).

Analysis of shield elemental composition

Complete ventro-caudal shields were dissected from three individuals of *S. chinensis* and three of *S. liui* syn. n. Sediment organic contaminations were removed by first cleaning the shields with a soft brush, then rinsing with distilled water, soaking in sodium hypochlorite (10 vol%) for 10 min, ultrasonic cleaning, and air-dried.

Cleaned shields were trimmed, polished to 10–30-µm thick using lapping machine and polishing machine, and sputter-coated with carbon using a JEE-420 vacuum evaporator (JEOL Ltd., Japan) for electron probe microanalysis (EPMA), which were performed with the electron probe analyzer JOEL JXA-8230 at the Marine Geology and Geophysics Lab of the First Institute of Oceanography (Ministry of Natural Resources, China). As shields are not formed by chitin (Goodrich, 1897), the carbon coating acted as the conductive media without influencing the analysis. The accelerating voltage was set to 15 kV with a beam current of 10 nA and a beam diameter of 1 µm.

Based on results of previous shield element analyses (Lowenstam, 1972) and our total element qualitative analyses, Iron (Fe), phosphorus (P), calcium (Ca), magnesium (Mg) and manganese (Mn), nitrogen (N) and sulfur (S) and silicon (Si) were selected for quantitative analyses. Eight random points per shield and three shields for each morphotype (n = 8 × 3) were chosen for element quantified analyses. Student's t-test (SPSS 26.0 software IBM SPSS Inc., USA) allowed comparing each element distribution [as mean ± standard deviation (SD)] between two morphotypes, which were plotted with Origin 9.5 (Origin Lab, USA). Backscattered electron (BSE) image intensity indicating the mean atomic number was used to locate the

compositional differences (Llovet et al., 2021). EPMA maps showing individual element distribution in shields were obtained for microscopic, local, and lateral shields by scanning with beam diameters of 0.3, 1, and 3 μm, respectively.

RNA extraction, sequencing, and bioinformatic analyses

Total RNA was extracted from the body wall around shields of five specimens of *S. chinensis* and five specimens of *S. liui* syn. n using MicroElute Total RNA Kit (OMEGA, USA) according to manufacturer's instructions. RNA quantity and quality were evaluated using a NanoDrop 2000 (Thermo Scientific, USA) and a Bioanalyzer 2100 (Agilent Technologies, USA). The cDNA libraries were prepared using the TruSeq RNA Library Prep Kit (Illumina, USA) and then sequenced on an Illumina HiSeq2000 sequencer to produce 150-bp paired-end reads at Shanghai OE Biotech Co., Ltd. (China).

Adaptors and low-quality Illumina reads were filtered using Trimmomatic v0.36 (Bolger et al., 2014) under the default parameters. To compare the two morphotypes' gene expression profiles, we assembled their RNA sequencing (RNAseq) data (Sandoval-Castillo et al., 2020). All clean reads were *de novo* assembled using Trinity v2.4.0 (Grabherr et al., 2011) under the default settings. The longest isoform from each gene was selected as "unigene," and the redundancy was eliminated using CD-HIT v4.8.1 with 95% similarity (Li et al., 2001). Unigenes were annotated using Diamond BLASTx v2.0.14 (Buchfink et al., 2015) with an E-value threshold of $1e^{-5}$ against the NCBI NR, Swiss-Port, euKaryotic Orthologous Groups (KOG), Gene Ontology (GO), eggNOG, and Kyoto Encyclopedia of Genes and Genomes (KEGG). The protein family for each unigene was determined using HMMER 3.3.2 (Mistry et al., 2013) against the Pfam database with an E-value threshold of $1e^{-5}$.

Gene expression levels were determined using Bowtie2 (Langmead and Salzberg, 2012). The results were normalized as transcripts per kilobase of exon model per million mapped reads (FPKM) (Trapnell et al., 2010). Principal component analysis (PCA; visualized using the R package PCAtools v2.5.13) allowed comparing the gene expression profiles among morphotypes and individuals. Differentially expressed genes (DEGs) between the two morphotypes were determined using DESeq (Anders and Huber, 2012). Only unigenes with $\log_2$fold change >1 and a *p*-value <0.05 were selected. GO and KEGG enrichment analyses of DEGs were conducted using Goseq R and KOBAS software packages, respectively (Kanehisa et al., 2007; Young et al., 2010). DEG heatmap and volcano plot were created using the R package pheatmap and ggplot, respectively.

Differential biomineralization mechanisms in *S. chinensis* and *S. liui* syn. n were revealed by identifying the putative biomineralization-related genes by BLASTx-identified DEGs against the Shell Matrix Protein (SMP) database (https://doi.org/10/cz2w) with a threshold of E-value $1e^{-10}$ and a >50% identity (Altschul et al., 1997). The correlation heatmap was created using the R package ComplexHeatmap v2.11.1.

Real-time PCR validation

Gene expression profiles were validated using real-time polymerase chain reaction (RT-PCR) analysis. Five representative SMP-like DEGs were selected, and the corresponding primers were designed using the online NCBI primer-BLAST tool (Table S4). The identical RNA samples were used for RT-PCR and RNAseq analyses, and cDNA was synthesized from 0.5 μg of DNase-treated RNA using TransScript First-Strand cDNA Synthesis SuperMix (TransGen Biotech, China). RT-PCR was performed on an ABI7500 instrument (Applied Biosystems, USA) with SYBR®Green (Applied Biosystems, USA) with three technical replicates per individual and three individuals for each morphotype. A three-step method was employed for RT-PCR amplification. The annealing temperature was done at 58°C. Relative expression levels were calculated using the $2^{-\triangle\triangle Ct}$ method (Livak and Schmittgen, 2001), with the mean expression levels of *18S* and *α-tubulin* being used as references. Expression profiles and Pearson correlation coefficient between RT-PCR and RNAseq were calculated and visualized using GraphPad Prism 8.

Results

Synonymy of *S. chinensis* with *S. liui* syn. n based on DNA barcoding and mitogenomes

The interspecific uncorrected *p* distance (0–0.007) of *COI*, *16S*, and the nuclear *18S* and *28S* markers between *S. chinensis* and *S. liui* syn. n was at least one order of magnitude smaller than that of between other species but was equivalent to their intraspecific genetic distance (0–0.009, Table S5), suggesting that they might be genetically identical (Drennan et al., 2019).

The mitogenome size of *S. chinensis*, *S. liui* syn. n, *S. sendalli*, and *S. buzhinskajae* ranged from 15,287 to 17,728 bp (Table S6) and contained 13 PCGs, two rRNAs, and 22 tRNAs. Their gene orders were the same, while the order of the 13 PCGs was conserved with the putative ground pattern of Pleistoannelida (Weigert et al., 2015), except for the translocation of NADH-ubiquinone oxidoreductase chain 1 (*nad1*) (Figure S5).

The four sternaspids showed a monophyletic relationship (Figure 2). *Sternaspis liui* syn. n and *S. chinensis* had a branch length close to 0 (Figure 2), mitochondrial genomes with a 99.9% sequence similarity (Table S7), and paired nucleotide distances

for the 13 PCGs and the two rRNAs ranging from 0 to 0.002 (Table S8), supporting that the former should be a junior synonym of the latter despite having two morphotypes.

Elements

Fe, P, Ca, Mg, and Mn were significantly more abundant in *S. chinensis* than in *S. liui* syn. n, while N and S were significantly less abundant (Figure 3; Figures S6, S7). The distribution of these elements was relatively uniform in *S. chinensis* and heterogeneous in *S. liui* syn. n (Figures S6, S7). N and S, which might represent proteins, were more abundant in the areas with low contents of Fe, P, Ca, Mg, and Mn in *S. liui* syn. n (Figure S6). The two shield types showed higher abundances of Fe, P, and Ca in the central shield area, with external radiation strip regions (Figure 4), which corresponded to the ribs on the shield surface (Figures S1, S2). Notably, a polygonal microstructure was found in the shields of the two shield types (Figure 5, Figure S6B), with the highest Fe, P, and Ca contents at the edge, intermediately inward, and zero-areas scattered inside (Figure 5). This structure occurred in the whole shield of *S. chinensis* but only in the central with radiation strip regions with high Fe, P, and Ca contents in *S. liui* syn. n (Figure 5, Figure S6).

Transcriptomes

The body wall around the shield of the two morphotypes produced 493.39 million clean reads (49.34 million reads per individual on average) (Table S9). *De novo* assembly resulted in 128,181 unigenes with an N50 of 1,146 bp and a GC content of 40.11%. These unigenes were successfully annotated with any of the seven protein databases (Tables S10, S11).

The first axis of the PCA accounted for 77.49% of variations and allowed to clearly distinguish the two morphotypes, while they showed a strong clustering for the individual samples (Figure 6A). The mitochondrial genes cytochrome b (*cob*) and NADH dehydrogenase subunit 2 (*nad2*) that showed a high loading in PCI (Figure 6B) were highly expressed in *S. liui* syn. n, while the genes encoding actin-related protein (*arp*) and myosin regulatory light chain (*mrlc*) with high loading in PCI exhibited a high expression in *S. chinensis* (Figure 6B).

Sternaspis chinensis and *S. liui* syn. n showed 17,751 DEGs, with 6,503 and 11,248 upregulated genes, respectively (Figures 6C, D). Upregulated genes in *S. chinensis* were mainly annotated GO terms related to biomineralization (ion transport and calmodulin binding) (Figure 7). While upregulated genes in *S. liui* syn. n were associated with protein synthesis and energy

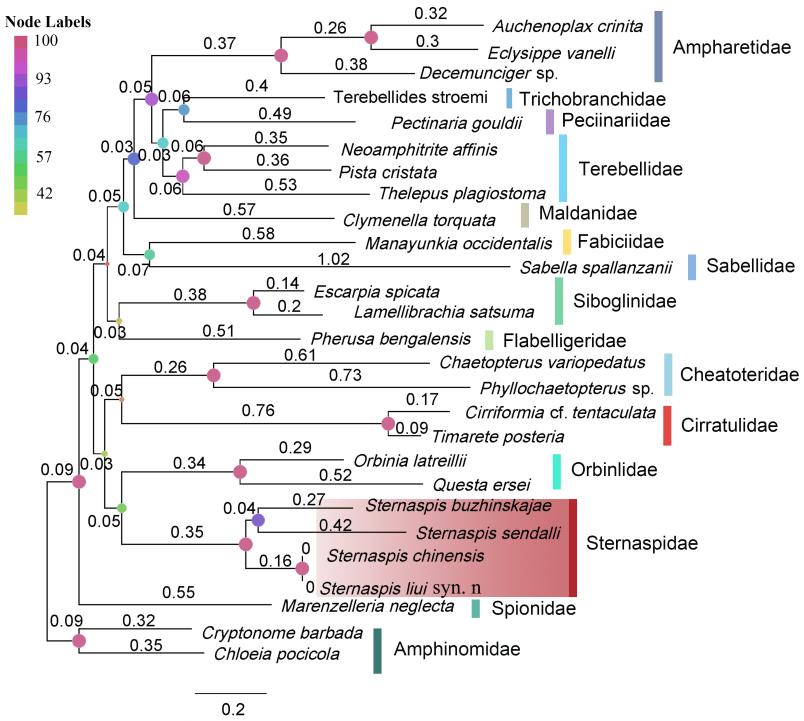

FIGURE 2
Maximum-likelihood tree based on nucleotide sequences of 13 PCGs and two rRNAs. The node labels indicated bootstrap supports. Branch lengths are indicated above the branch.

10.3389/fmars.2022.984989

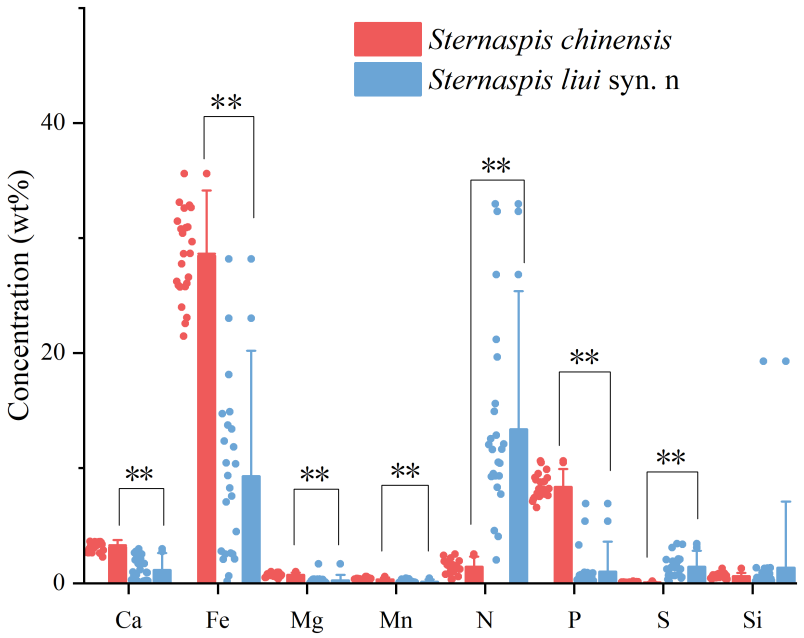

FIGURE 3
Comparison of the main element contents in the ventro-caudal shields of the two sternaspid morphotypes. Bars: mean ± SD (n = 24). Double asterisk (**) above the bars represents a significant difference between the two synonymous species ($p < 0.01$, Student's t-test).

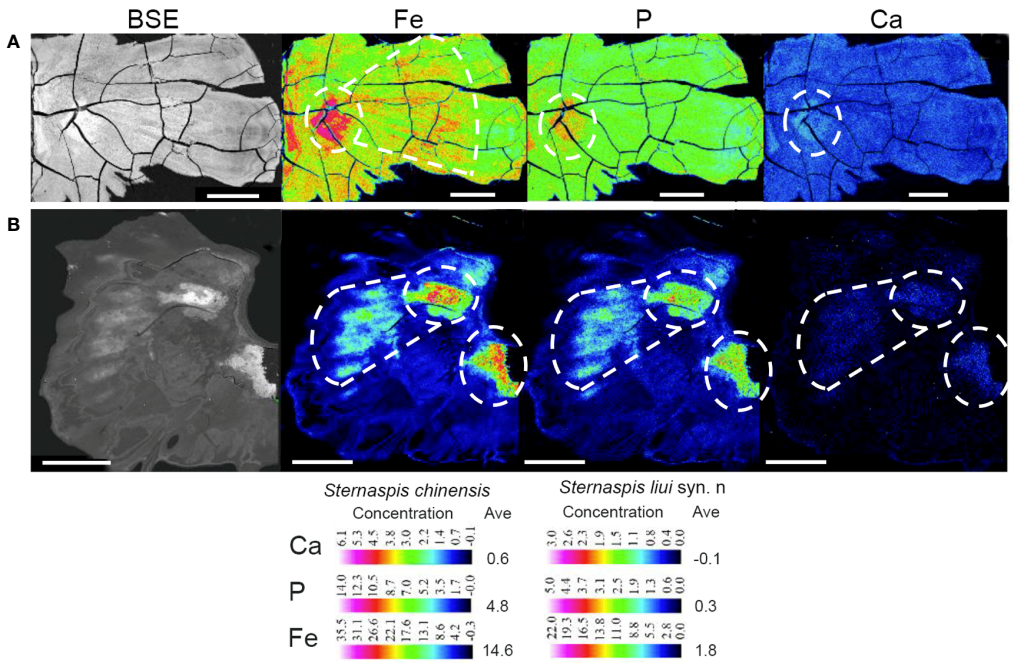

FIGURE 4
Backscattered electron (BSE) images and electron probe microanalysis (EPMA) elemental maps of Fe, P, and Ca in shield plates of **(A)** *Sternaspis chinensis* and **(B)** *Sternaspis liui* syn. n. Ave, average concentration. BSE image scale bar: 100 μm; Fe, P, and Ca EPMA map scale bar: 500 μm. White circles, high element abundance.

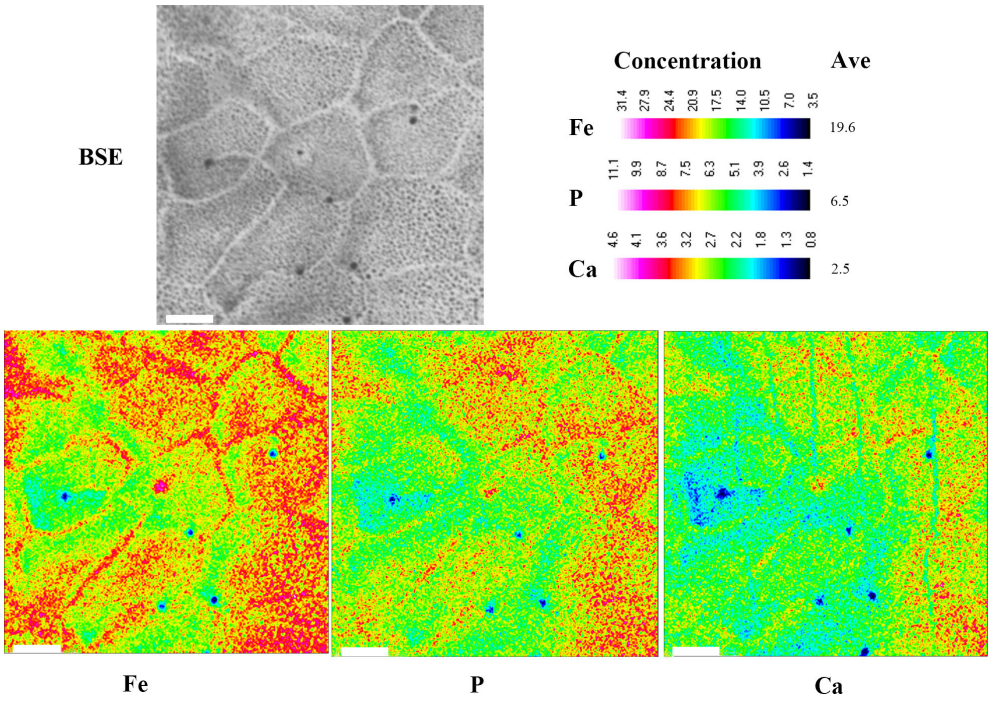

FIGURE 5
Backscattered electron (BSE) images and electron probe microanalysis (EPMA) elemental maps of Fe, P, and Ca for *Sternaspis chinensis*. Ave, average concentration. Scale bar: 10 μm.

production (respiratory chain, respiratory chain complex III, and cytosolic large/small ribosomal subunits) (Figure 7). In addition, shield formation-related pathways (calcium signaling and pantothenate and coenzyme A (CoA) biosynthesis) were enriched in *S. chinensis* and transcription and energy metabolism-related pathways (ribosome and oxidative phosphorylation) in *S. liui* syn. n (Figure S8).

Biomineralization-related differentially expressed genes and proteins

Among the two sternaspid morphotypes, a total of 24 DEGs were identified as SMP-related genes through the homolog search against an SMP database, including two BPTI/Kunitzs, nine Cyclophilin PPIases, one Filament/Filmin, eight fructose–bisphosphate aldolase (FBPA), one Glycoside hydrolase, Peroxiredoxin, and two Transgelin-Calponin (Table S12). Six of them were highly expressed in *S. chinensis*, and 18 SMP-related genes were actively transcribed in *S. liui* syn. n (Figure 8, Table S12). FBPA, Transgelin-Calponin, and BPTI/Kunitzs were highly expressed in both morphotypes (Figure 8).

Gene expression validation by RT-PCR

Five DEGs possibly related to shield formation were selected for RT-PCR analysis: two encoding SMPs (FBPA and transgelin-calponin), two of chitin synthesis-related GO terms (chitin-based embryonic cuticle biosynthetic process and chitin synthase activity), and one of heat shock protein (Table S4). Their $\log_2$fold change values in RT-PCR and RNAseq were significantly correlated (R^2 = 0.89, $p < 0.05$), and all of them were upregulated in both data in *S. chinensis* compared to *S. liui* syn. n (Figure S9), implying the high quality of our transcriptome data.

Discussion

Shield morphological variation and chemical composition

Sternaspis chinensis and *S. liui* syn. n were originally described based on morphological features (Wu et al., 2015), including the shields. In *S. liui* syn. n, they are soft, with prominent ribs and concentric lines near the margin, while in *S. chinensis*, they are stiff, with flat ribs and concentric lines (Wu

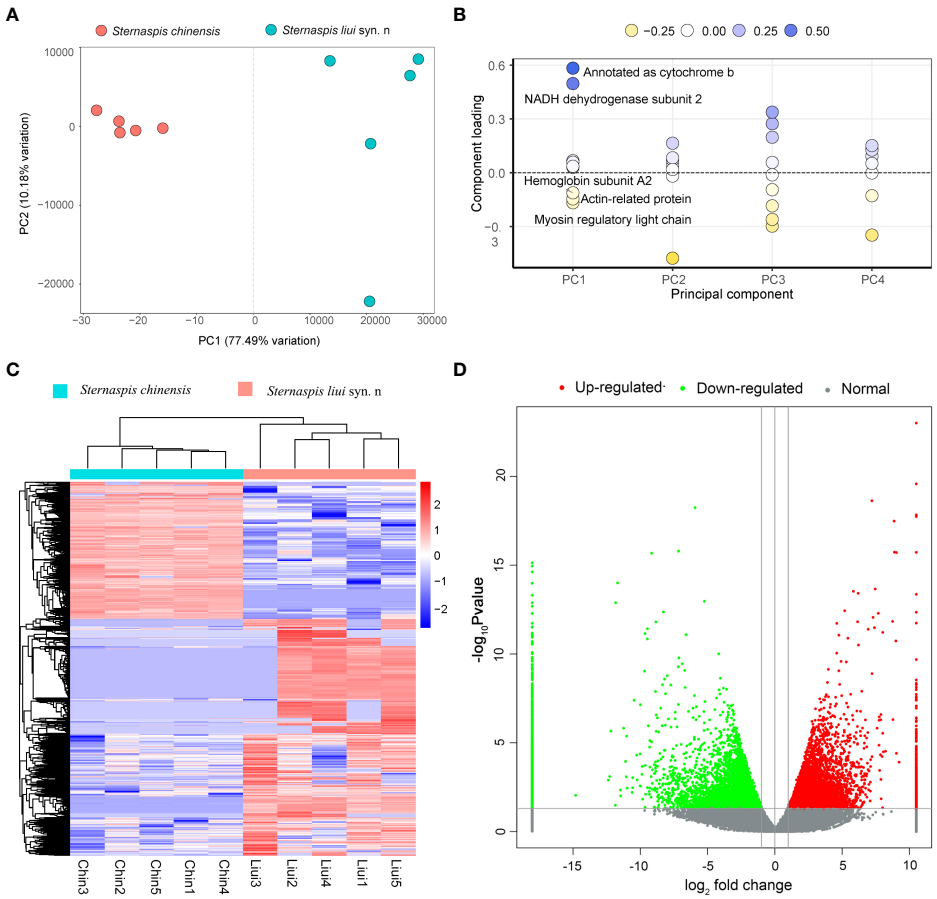

FIGURE 6
Comparative analysis of gene expression. **(A)** PCA for all genes. **(B)** Loading plot of the first five principal components. **(C)** Heatmap showing the profiles of the differentially expressed genes (DEGs) (red, upregulated; blue, downregulated). **(D)** DEG volcano plot. DEGs were filtered by *p*-value <0.05 and |$\log_2$fold change| >1.

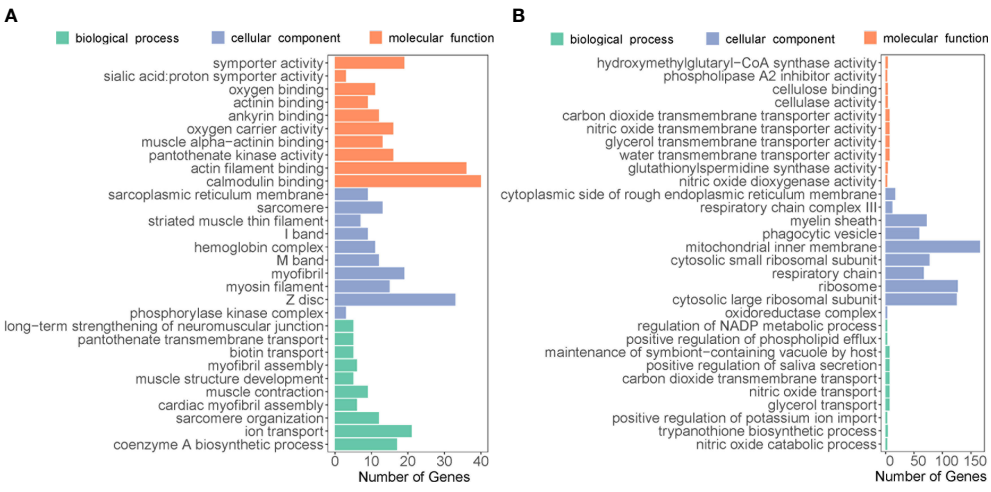

FIGURE 7
Top 30 enriched Gene Ontology categories associated with upregulated genes in **(A)** *Sternaspis chinensis* and **(B)** *Sternaspis liui* syn. n.

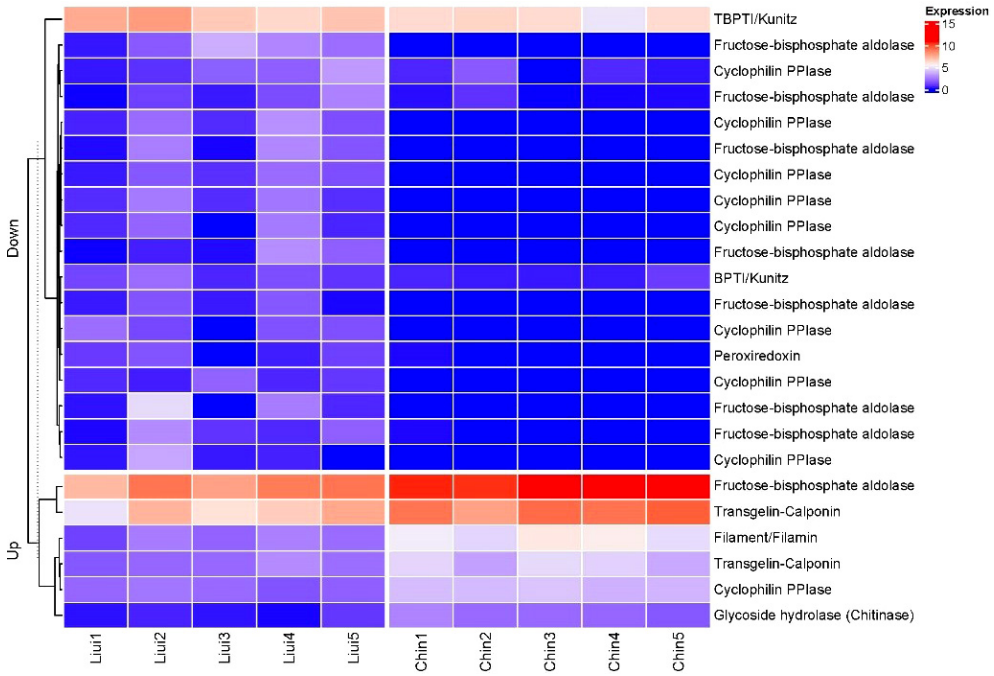

FIGURE 8
Heatmap of the hierarchical clustering showing the profiles for the SMP-related differentially expressed genes. Expression: $\log_2$(FPKM+1); Up, upregulated genes in *Sternaspis chinensis vs. Sternaspis liui* syn. n; Down, downregulated genes in *S. chinensis vs. S. liui* syn. n; Liui1–5, specimens of *S. liui* syn. n; Chin1–5, specimens of *S. chinensis*.

et al., 2015). However, we have demonstrated that these two species are genetically identical, with 0–0.007 pairwise genetic distances for *COI*, *16S*, *18S*, and *28S*. The monophyletic relationship, low branch length, and intraspecies level genetic distance based on mitogenomes clearly support that the two morphotypes correspond to synonyms instead of species. Therefore, shield examination and molecular evidence must be integrated into the taxonomic diagnosis of sternaspids, as postulated by Drennan et al. (2019). However, whether they are the two ecotypes of *S. chinensis* including the genetic variations of the two populations needs to be further analyzed using nuclear DNA single nucleotide polymorphisms (SNPs).

The shield elemental compositions of the two morphotypes revealed Fe, P, and Ca as being higher in *S. chinensis* than in *S. liui* syn. n. The hardness of the sternaspid shield seemed to be determined by the abundance of mineralized Fe (Bartolomaeus, 1992), which might imply a higher level of shield biomineralization and stiffness in *S. chinensis* than *in S. liui* syn. n. Variations in structure and composition of biominerals are also common in mollusks, usually in association with the environmental condition and fostering local adaptations (Hoffman et al., 2009; Zieritz et al., 2010). Iron sulfide contents in the sclerites of scaly-foot snails were positively correlated with its environmental concentration, likely being a detoxication mechanism (Nakamura et al., 2012), while water chemistry and food and nutrient supply highly impacted the shell production in the blue mussel *Mytilus edulis* (Michalek, 2019). Therefore, variations in shield element contents in the two morphotypes might be related to their living environments, although further detailed analysis of the elemental composition of their habitats is required to evaluate this hypothesis.

The mechanical properties of the biominerals can be affected by many factors, including chemical composition, microstructure, and organic matrix embedded in the minerals (Marcus et al., 2017; Bianco-Stein et al., 2020; Yamagata et al., 2022). Herein, Fe, P, and Ca are critical elements of shield components, distributed as polygonal microstructures in the whole shield of *S. chinensis* but only in the center with radiation strip regions in *S. liui* syn. n (Figure 5, Figure S6). The polygonal microstructure is commonly found with various functions in skeletons of marine organisms, such as strengthening hardness and lightening weight in sea urchin *Cidaris rugosa* exoskeleton and changing body color in polychaete *Aphrodita aculeata* spines (Murray, 2018). Furthermore, the polygonal microstructure proved to be excellent in economizing materials because hexagonal cells require the least total wall length when filling a flat plane (Murray, 2018). However, the interrelationship between the chemical composition, microstructure, and mechanical properties especially shield hardness needs further exploration.

Differential gene expression

The divergent shield biomineralization shown by the two morphotypes may be associated with their differential gene regulation, especially in biomineralization-related gene expression. Two mitogenes (*cob* and *nad2*) identified in PCA were highly expressed in *S. liui* syn. n, which may be a reflection of the difference in energy metabolism involved in biological processes, including biomineralization. Mitogenes are involved in complex bioenergetic pathways helping marine animals cope with disturbances by phenotype selection, habitat translocations, and responses to climate-related conditions. Some mitogenes in the mantle of *Mytilus chilensis* from two different habitats played key roles in its adaptive responses to biomineralization, feeding, and locomotion (Yévenes et al., 2022). The other two genes identified in PCA actively transcribed in *S. chinensis* were *mrlc* and *arp*, which may foster a high level of shield biomineralization. The former is a calcium-binding protein with the SMP-related EF-hand domain that is involved in shell formation (Guan et al., 2017), while the latter could control biomineralization by forming dynamic scaffolds and templates (Tyszka et al., 2019).

A large number of DEGs and GO enrichments between the two sternaspid morphotypes showed their unique physiological functions. Given that tissues around the shield may play multiple functions, these differential expressions were not just representative biomineralization-specific genes. For *S. chinensis*, the enriched ion transport (Yarra et al., 2021) and calmodulin binding (Yan et al., 2007; Fang et al., 2008; Mao et al., 2019) were suspected to be associated with hypothetical biomineralization pathways. Compared with *S. chinensis*, the transcripts of *S. liui* syn. n has more upregulated DEGs involved in energy metabolism and protein synthesis. For example, 1) "respiratory chain" and "respiratory chain complex III" are protein complexes forming electron transport systems, highly expressed in the mineralized teeth region of *Cryptochiton stelleri*, providing the energy for iron transport required for mineralization (Nemoto et al., 2019), and 2) "cytosolic large/small ribosomal subunits" are the places for intracellular protein synthesis (Brar and Weissman, 2015). Although mitochondrial and ribosomal genes are not biomineralization genes, they were among the most abundantly expressed in the mollusk mantles that is the shell formation tissue (Shi et al., 2013; Shi et al., 2019).

Proteins involved in differential biomineralization

Seven SMP-related proteins involved in molluskan biomineralization were annotated from the DEGs of the two sternaspid morphotypes (Figure 8). These proteins contained some key biomineralization domains, for example, Glyco_18, CH (Calponin homology domain), IG_FLMN (Filamin-type immunoglobulin domain), KU (BPTI/Kunitz family of serine protease inhibitors domain), and TIL (Trypsin Inhibitor like cysteine-rich domain) (Table S12) (Liao et al., 2021; Yarra et al., 2021). The genes coding FBPA and cyclophilin PPIase were differentially expressed in the two morphotypes (Figure 7). These two proteins proved to have multiple biological functions not limited to biomineralization. Thus, they could invoke different expression profiles in the two morphotypes. FBPA containing glycolytic domain plays a role in the stabilization of amorphous calcium carbonate in crustacean exoskeleton mineralization (Sato et al., 2011; Abehsera et al., 2018), participates in carbohydrate metabolism, and provides energy for the organism (Guo et al., 2010; Di et al., 2017). Cyclophilins with pro_isomerase domain was found to be integral to primary mesenchymal sea urchin cells as well as protein folding (Wilt and Killian, 2008; Manno et al., 2012; Nemoto et al., 2012).

Protease inhibitor BPTI/kunitz and peroxiredoxin were actively transcribed in this junior synonym species. Protease inhibitors with KU and TIL domains are common mollusk shell matrix proteins, having an inhibitory function on biomineralization (Y.-J. Rose-Martel et al., 2015; Luo, 2017; Takeuchi et al., 2021). Peroxiredoxin is involved in the reduction of iron oxide in the mineralized cusp of chiton teeth (Kisailus and Nemoto, 2018). Therefore, their expression in *S. liui* syn. n might contribute to the biomineralization process.

The SMP-related proteins chitinase, transgelin-calponin, and filament/filamin were highly expressed in *S. chinensis* (Figure 8). Chitinase with the conserved Glyco_18 domain is an enzyme that hydrolyzes chitin oligosaccharides (Zhang et al., 2019; Liao et al., 2021; Liu et al., 2021) and participates in the formation of the metazoan chitin scaffold (Le Pabic et al., 2017). Calponin with the CH domain is an important protein involved in calcification in mollusks and branchiopods (Y. J. Luo et al., 2015; Sun et al., 2021). Filamin proteins with CH and IG_FLMN domains in humans and pearl oysters could interact with the calcium-sensing receptor and promote the calcification Rho signaling pathway (Awata et al., 2001; Pi et al., 2002; Matsuura et al., 2018). Therefore, these upregulated genes might contribute to the high shield biomineralization level in *S. chinensis*, while the differential expression of protease inhibitors with the function of biomineralization inhibition between the two morphotypes might govern their differential levels in biomineralization.

Conclusion

This study proved that *S. liui* syn. n is, in fact, a junior synonym of *S. chinensis*. Shield biomineralization in these two morphotypes of synonymous species has been revealed by composition and structure analysis, showing the natural formation of a polygonal microstructure composed of ferric phosphate hydrogels. Our study also showed that higher abundance of Fe, P, and Ca in *S. chinensis* shield corresponds to more polygonal microstructures than that in *S. liui* syn. n. Transcriptome analyses provided insights into the respective biomineralization molecular mechanism, suggesting that *S. chinensis* exhibited higher biomineralization activities, especially high expression of some SMP-related proteins (i.e., calponin, filamin, chitinase) resulting in a high level of shield biomineralization. *Sternaspis chinensis*. syn. n exhibited a high expression of energy mechanism-related genes and encoding protease inhibitor genes, reflecting its low level of biomineralization. Overall, our findings enhance the understanding of the mechanisms underlying biomineralization in sternaspids, with chemical and molecular data generated being also useful for further studies on the evolution of the mineralization process in polychaete annelids.

Data availability statement

The datasets presented in this study can be found in online repositories. The names of the repository/repositories and accession number(s) can be found in the article/ Supplementary Material.

Author contributions

QX and MG conceived and designed the original research, wrote the initial manuscript. MG and JM analyzed the data. YL and WS collected samples and help interpret the data. JI, QX, ZW and XZ revised and approved the manuscript. All authors contributed to the article and approved the submitted version.

Funding

This study was supported by the foundation of the National Natural Science Foundation of China (42176135, 4181101341).

Acknowledgments

We thank the captains, crews and operation teams of the research vessels "Xiangyanghong 01" and "Xiangyanghong 18" for collecting the samples. We thank Dr. Xuwen Wu for his guidance on morphological identification of sternaspids. We acknowledge the Lab of Marine Geology and Geophysics of First Institute of Oceanography, Ministry of Natural Resources for electron probe microanalysis. We are grateful to the previous reviewers for their constructive suggestions for this paper and corrections of language.

Conflict of interest

The authors declare that the research was conducted in the absence of any commercial or financial relationships that could be construed as a potential conflict of interest.

Publisher's note

All claims expressed in this article are solely those of the authors and do not necessarily represent those of their affiliated organizations, or those of the publisher, the editors and the reviewers. Any product that may be evaluated in this article, or claim that may be made by its manufacturer, is not guaranteed or endorsed by the publisher.

Supplementary material

The Supplementary Material for this article can be found online at: https://www.frontiersin.org/articles/10.3389/fmars.2022.984989/full#supplementary-material

References

Abehsera, S., Weil, S., Manor, R., and Sagi, A. (2018). The search for proteins involved in the formation of crustacean cuticular structures. *Hydrobiologia* 825, 29–45. doi: 10.1007/s10750-018-3684-y

Altschul, S. F., Madden, T. L., Schäffer, A. A., Zhang, J., Zhang, Z., Miller, W., et al. (1997). Gapped blast and psi-blast: A new generation of protein database search programs. *Nucleic Acids Res.* 25, 3389–3402. doi: 10.1093/nar/25.17.3389

Anders, S., and Huber, W. (2012). Differential expression of rna-seq data at the gene level–the deseq package. *Heidelberg Germany: Eur. Mol. Biol. Lab. (EMBL)* 10, f1000research.

Andrews, S. (2010). *Fastqc: A quality control tool for high throughput sequence data*. Available at: http://www.bioinformatics.babraham.ac.uk/projects/fastqc

Awata, H., Huang, C., Handlogten, M. E., and Miller, R. T. (2001). Interaction of the calcium-sensing receptor and filamin, a potential scaffolding protein. *J. Biol. Chem.* 276, 34871–34879. doi: 10.1074/jbc.M100775200

Bartolomaeus, T. J. M. M. (1992). On the ultrastructure of the cuticle, the epidermis and the gills of *sternaspis* scutata (annelida). *Microfauna Marina* 7, 237–252.

Bernt, M., Donath, A., Jühling, F., Externbrink, F., Florentz, C., Fritzsch, G., et al. (2013). Mitos: Improved *de novo* metazoan mitochondrial genome annotation. *Mol. Phylogenet. Evol.* 69, 313–319. doi: 10.1016/j.ympev.2012.08.023

Bianco-Stein, N., Polishchuk, I., Seiden, G., Villanova, J., Rack, A., Zaslansky, P., et al. (2020). Helical microstructures of the mineralized coralline red algae determine their mechanical properties. *Adv. Sci. (Weinh)* 7, 2000108. doi: 10.1002/advs.202000108

Bolger, A. M., Lohse, M., and Usadel, B. (2014). Trimmomatic: A flexible trimmer for illumina sequence data. *Bioinformatics* 30, 2114–2120. doi: 10.1093/bioinformatics/btu170

Brar, G. A., and Weissman, J. S. (2015). Ribosome profiling reveals the what, when, where and how of protein synthesis. *Nat. Rev. Mol. Cell Biol.* 16, 651–664. doi: 10.1038/nrm4069

Buchfink, B., Xie, C., and Huson, D. H. (2015). Fast and sensitive protein alignment using diamond. *Nat. Methods* 12, 59–60. doi: 10.1038/nmeth.3176

Clark, M. S. (2020). Molecular mechanisms of biomineralization in marine invertebrates. *J. Exp. Biol.* 223, jeb206961. doi: 10.1242/jeb.206961

Di, G., Kong, X., Miao, X., Zhang, Y., Huang, M., Gu, Y., et al. (2017). Proteomic analysis of trochophore and veliger larvae development in the small abalone *haliotis diversicolor*. *BMC Genomics* 18, 809. doi: 10.1186/s12864-017-4203-7

Drennan, R., Wiklund, H., Rouse, G. W., Georgieva, M. N., Wu, X., Kobayashi, G., et al. (2019). Taxonomy and phylogeny of mud owls (annelida: Sternaspidae), including a new synonymy and new records from the southern ocean, north east atlantic ocean and pacific ocean: Challenges in morphological delimitation. *Mar. Biodiversity* 49, 2659–2697. doi: 10.1007/s12526-019-00998-0

Fang, Z., Yan, Z., Li, S., Wang, Q., Cao, W., Xu, G., et al. (2008). Localization of calmodulin and calmodulin-like protein and their functions in biomineralization in *p. fucata*. *Prog. Natural Sci.* 18, 405–412. doi: 10.1016/j.pnsc.2007.11.011

Fiege, D., and Barnich, R. (2020). A new genus and species of sternaspidae (annelida: Polychaeta) from the deep eastern atlantic. *Eur. J. Taxonomy* 699, 1–13. doi: 10.5852/ejt.2020.699

Goodrich, E. (1897). Memoirs: Notes on the anatomy of sternaspis. *Q. J. Microscopical Sci.* 40, 233–245. doi: 10.1242/jcs.s2-40.158.233

Grabherr, M. G., Haas, B. J., Yassour, M., Levin, J. Z., Thompson, D. A., Amit, I., et al. (2011). Trinity: Reconstructing a full-length transcriptome without a genome from rna-seq data. *Nat. Biotechnol.* 29, 644. doi: 10.1038/nbt.1883

Guan, Y., He, M., and Wu, H. (2017). Differential mantle transcriptomics and characterization of growth-related genes in the diploid and triploid pearl oyster *pinctada fucata*. *Mar. Genomics* 33, 31–38. doi: 10.1016/j.margen.2017.01.001

Guo, D., Keightley, A., Guthrie, J., Veno, P. A., Harris, S. E., and Bonewald, L. F. (2010). Identification of osteocyte-selective proteins. *Proteomics* 10, 3688–3698. doi: 10.1002/pmic.201000306

Heffernana1, P. (1990). Ultrastructural studies of the elytra of *pholoe minuta* (annelida: Polychaeta) with special reference to functional morphology. *J. Mar. Biol. Assoc. United Kingdom* 70, 545–556. doi: 10.1017/S0025315400036572

Hoffman, J. I., Peck, L. S., Hillyard, G., Zieritz, A., and Clark, M. S. (2009). No evidence for genetic differentiation between antarctic limpet *nacella concinna* morphotypes. *Mar. Biol.* 157, 765–778. doi: 10.1007/s00227-009-1360-5

Jin-Bao, W., Xin-Zheng, L., and Hong-Fa, W. (2006). Ecological characteristics of dominant polychaete species from the jiaozhou bay. *Curr. Zool* 52, 63–70. doi: 10.3969/j.issn.1674-5507.2006.01.007

Kanehisa, M., Araki, M., Goto, S., Hattori, M., Hirakawa, M., Itoh, M., et al. (2007). Kegg for linking genomes to life and the environment. *Nucleic Acids Res.* 36, D480–D484. doi: 10.1093/nar/gkm882

Kisailus, D., and Nemoto, M. (2018). *Structural and proteomic analyses of iron oxide biomineralization in chiton teeth biological magnetic materials and applications* (Singapore: Springer), 53–73. doi: 10.1007/978-981-10-8069-2_3

Kumar, S., Stecher, G., and Tamura, K. (2016). Mega7: Molecular evolutionary genetics analysis version 7.0 for bigger datasets. *Mol. Biol. Evol.* 33, 1870–1874. doi: 10.1093/molbev/msw054. evolution.

Langmead, B., and Salzberg, S. L. (2012). Fast gapped-read alignment with bowtie 2. *Nat. Methods* 9, 357–359. doi: 10.1038/nmeth.1923

Le Pabic, C., Marie, A., Marie, B., Percot, A., Bonnaud-Ponticelli, L., Lopez, P. J., et al. (2017). First proteomic analyses of the dorsal and ventral parts of the *sepia officinalis* cuttlebone. *J. Proteomics* 150, 63–73. doi: 10.1016/j.jprot.2016.08.015

Liao, Q., Qin, Y., Zhou, Y., Shi, G., Li, X., Li, J., et al. (2021). Characterization and functional analysis of a chitinase gene: Evidence of ch-chit participates in the regulation of biomineralization in *crassostrea hongkongensis*. *Aquaculture Rep.* 21, 100852. doi: 10.1016/j.aqrep.2021.100852

Li, W., Jaroszewski, L., and Godzik, A. (2001). Clustering of highly homologous sequences to reduce the size of large protein databases. *Bioinformatics* 17, 282–283. doi: 10.1093/bioinformatics/17.3.282

Liu, C., Ji, X., Huang, J., Wang, Z., Liu, Y., and Hincke, M. T. (2021). Proteomics of shell matrix proteins from the cuttlefish bone reveals unique evolution for cephalopod biomineralization. *ACS Biomaterials Sci. Eng.* 2373–9878, 1–12. doi: 10.1021/acsbiomaterials.1c00693

Livak, K. J., and Schmittgen, T. D. (2001). Analysis of relative gene expression data using real-time quantitative pcr and the $2^{-\delta\delta ct}$ method. *Methods* 25, 402–408. doi: 10.1006/meth.2001.1262

Llovet, X., Moy, A., Pinard, P. T., and Fournelle, J. H. (2021). Reprint of: Electron probe microanalysis: A review of recent developments and applications in materials science and engineering. *Prog. Materials Sci.* 120, 100818. doi: 10.1016/j.pmatsci.2021.100818

Lowenstam, H. A. (1972). Phosphatic hard tissues of marine invertebrates: Their nature and mechanical function, and some fossil implications. *Chem. Geology* 9, 153–166. doi: 10.1016/0009-2541(72)90053-8

Luo, Y.-J. (2017). *Insights into lophotrochozoan evolution and the origin of morphological novelties from brachiopod, phoronid, and nemertean genomes*. PhD Thesis. Okinawa Institute of Science and Technology Graduate University.

Luo, Y. J., Takeuchi, T., Koyanagi, R., Yamada, L., Kanda, M., Khalturina, M., et al. (2015). The *lingula* genome provides insights into brachiopod evolution and the origin of phosphate biomineralization. *Nat. Commun.* 6, 8301. doi: 10.1038/ncomms9301

Malachowicz, M., and Wenne, R. (2019). Mantle transcriptome sequencing of mytilus spp. and identification of putative biomineralization genes. *PeerJ* 6, e6245. doi: 10.7717/peerj.6245

Manno, D., Carata, E., Tenuzzo, B. A., Panzarini, E., Buccolieri, A., Filippo, E., et al. (2012). High ordered biomineralization induced by carbon nanoparticles in the sea urchin *paracentrotus lividus*. *Nanotechnology* 23, 495104. doi: 10.1088/0957-4484/23/49/495104

Mao, J., Zhang, W., Wang, X., Song, J., Yin, D., Tian, Y., et al. (2019). Histological and expression differences among different mantle regions of the yesso scallop (*patinopecten yessoensis*) provide insights into the molecular mechanisms of biomineralization and pigmentation. *Mar. Biotechnol.* 21, 683–696. doi: 10.1007/s10126-019-09913-x

Marcus, M. A., Amini, S., Stifler, C. A., Sun, C. Y., Tamura, N., Bechtel, H. A., et al. (2017). Parrotfish teeth: Stiff biominerals whose microstructure makes them tough and abrasion-resistant to bite stony corals. *ACS Nano* 11, 11856–11865. doi: 10.1021/acsnano.7b05044

Matsuura, A., Yoshimura, K., Kintsu, H., Atsumi, T., Tsuchihashi, Y., Takeuchi, T., et al. (2018). Structural and functional analyses of calcium ion response factors in the mantle of *pinctada fucata*. *J. Struct. Biol.* 204, 240–249. doi: 10.1016/j.jsb.2018.08.014

Michalek, K. (2019). *Scottish Mussel culture in the natural environment: Observations and implications for industry*. PhD Thesis. (University of Aberdeen).

Mistry, J., Finn, R. D., Eddy, S. R., Bateman, A., and Punta, M. (2013). Challenges in homology search: Hmmer3 and convergent evolution of coiled-coil regions. *Nucleic Acids Res.* 41, 121–121. doi: 10.1093/nar/gkt263

Murdock, D. J. E. (2020). The 'biomineralization toolkit' and the origin of animal skeletons. *Biol. Rev. Cambridge Philos. Soc.* 95, 1372–1392. doi: 10.1111/brv.12614

Murray, C. (2018). Patterns in nature: Why the natural world looks the way it does. *Crystallogr. Rev.* 24, 205–206. doi: 10.1080/0889311X.2018.1447569

Nakamura, K., Watanabe, H., Miyazaki, J., Takai, K., Kawagucci, S., Noguchi, T., et al. (2012). Discovery of new hydrothermal activity and chemosynthetic fauna on the central indian ridge at 18° -20°s. *PloS One* 7, e32965. doi: 10.1371/journal.pone.0032965

Nemoto, M., Ren, D., Herrera, S., Pan, S., Tamura, T., Inagaki, K., et al. (2019). Integrated transcriptomic and proteomic analyses of a molecular mechanism of radular teeth biomineralization in *cryptochiton stelleri*. *Sci. Rep.* 9, 856. doi: 10.1038/s41598-018-37839-2

Nemoto, M., Wang, Q., Li, D., Pan, S., Matsunaga, T., and Kisailus, D. (2012). Proteomic analysis from the mineralized radular teeth of the giant pacific chiton, *cryptochiton stelleri* (mollusca). *Proteomics* 12, 2890–2894. doi: 10.1002/pmic.201100473

Nguyen, L.-T., Schmidt, H. A., Von Haeseler, A., and Minh, B. Q. (2015). Iq-tree: A fast and effective stochastic algorithm for estimating maximum-likelihood phylogenies. *Mol. Biol. Evol.* 32, 268–274. doi: 10.1093/molbev/msu300

Nurk, S., Bankevich, A., Antipov, D., Gurevich, A., Korobeynikov, A., Lapidus, A., et al. (2013). Assembling genomes and mini-metagenomes from highly chimeric reads. *Res. Comput. Mol. Biol.* 7821, 158–170. doi: 10.1007/978-3-642-37195-0_13

Pi, M., Spurney, R. F., Tu, Q., Hinson, T., and Quarles, L. D. (2002). Calcium-sensing receptor activation of rho involves filamin and rho-guanine nucleotide exchange factor. *Endocrinology* 143, 3830–3838. doi: 10.1210/en.2002-220240

Rose-Martel, M., Smiley, S., and Hincke, M. T. (2015). Novel identification of matrix proteins involved in calcitic biomineralization. *J. Proteomics* 116, 81–96. doi: 10.1016/j.jprot.2015.01.002

Salazar-Vallejo, S. I., and Buzhinskaja, G. (2013). Six new deep-water sternaspid species (annelida, sternaspidae) from the pacific ocean. *Zookeys* 384, 1–27. doi: 10.3897/zookeys.348.5449

Sandoval-Castillo, J., Gates, K., Brauer, C. J., Smith, S., Bernatchez, L., and Beheregaray, L. B. (2020). Adaptation of plasticity to projected maximum temperatures and across climatically defined bioregions. *Proc. Natl. Acad. Sci. U. S. A.* 117, 17112–17121. doi: 10.1073/pnas.1921124117

Sato, A., Nagasaka, S., Furihata, K., Nagata, S., Arai, I., Saruwatari, K., et al. (2011). Glycolytic intermediates induce amorphous calcium carbonate formation in crustaceans. *Nat. Chem.* 7, 197–199. doi: 10.1038/nchembio.532

Sendall, K., and Salazar-Vallejo, S. I. (2013). Revision of sternaspis otto 1821 (polychaeta, sternaspidae). *Zookeys* 286, 1–74. doi: 10.3897/zookeys.286.4438

Shi, Y., Xu, M., Huang, J., Zhang, H., Liu, W., Ou, Z., et al. (2019). Transcriptome analysis of mantle tissues reveals potential biomineralization-related genes in *tectus pyramis* born. *Comp. Biochem. Physiol. Part D Genomics Proteomics* 29, 131–144. doi: 10.1016/j.cbd.2018.11.010

Shi, Y., Yu, C., Gu, Z., Zhan, X., Wang, Y., and Wang, A. (2013). Characterization of the pearl oyster (*pinctada martensii*) mantle transcriptome unravels biomineralization genes. *Mar. Biotechnol. (NY)* 15, 175–187. doi: 10.1007/s10126-012-9476-x

Sun, Y., Sun, J., Yang, Y., Lan, Y., Ip, J. C., Wong, W. C., et al. (2021). Genomic signatures supporting the symbiosis and formation of chitinous tube in the deep-sea tubeworm *paraescarpia echinospica*. *Mol. Biol. Evol.* 38, 4116–4134. doi: 10.1093/molbev/msab203

Takeuchi, T., Fujie, M., Koyanagi, R., Plasseraud, L., Ziegler-Devin, I., Brosse, N., et al. (2021). The 'shellome' of the crocus clam *tridacna crocea* emphasizes essential components of mollusk shell biomineralization. *Front. Genet.* 12, 674539. doi: 10.3389/fgene.2021.674539

Takeuchi, T., Yamada, L., Shinzato, C., Sawada, H., and Satoh, N. (2016). Stepwise evolution of coral biomineralization revealed with genome-wide proteomics and transcriptomics. *PloS One* 11, e0156424. doi: 10.1371/journal.pone.0156424

Tanur, A. E., Gunari, N., Sullan, R. M. A., Kavanagh, C. J., and Walker, G. C. (2010). Insights into the composition, morphology, and formation of the calcareous shell of the serpulid *hydroides dianthus*. *J. Struct. Biol.* 169, 145–160. doi: 10.1016/j.jsb.2009.09.008

Trapnell, C., Williams, B. A., Pertea, G., Mortazavi, A., Kwan, G., Van Baren, M. J., et al. (2010). Transcript assembly and quantification by rna-seq reveals unannotated transcripts and isoform switching during cell differentiation. *Nat. Biotechnol.* 28, 511–515. doi: 10.1038/nbt.1621

Tyszka, J., Bickmeyer, U., Raitzsch, M., Bijma, J., Kaczmarek, K., Mewes, A., et al. (2019). Form and function of f-actin during biomineralization revealed from live experiments on foraminifera. *Proc. Natl. Acad. Sci. U. S. A.* 116, 4111–4116. doi: 10.1073/pnas.1810394116

Vinn, O. (2021). Biomineralization in polychaete annelids: A review. *Minerals* 11, 1151. doi: 10.3390/min11101151

Vinn, O., Ten Hove, H. A., and Mutvei, H. (2008). On the tube ultrastructure and origin of calcification in sabellids (annelida, polychaeta). *Palaeontology* 51, 295–301. doi: 10.1111/j.1475-4983.2008.00763.x

Weigert, A., Golombek, A., Gerth, M., Schwarz, F., Struck, T. H., and Bleidorn, C. (2015). Evolution of mitochondrial gene order in annelida. *Mol. Phylogenet. Evol.* 94, 353–366. doi: 10.1016/j.ympev.2015.08.008

Wilt, F. H., and Killian, C. E. (2008). What genes and genomes tell us about calcium carbonate biomineralization. *Biomineralization: From Nat. to Appl.* 4, 36–69.

Wu, X., Salazar-Vallejo, S. I., and Xu, K. (2015). Two new species of sternaspis otto 1821 (polychaeta: Sternaspidae) from china seas. *Zootaxa* 4052, 373–382. doi: 10.11646/zootaxa.4052.3.7

Yamagata, N., Randall, G., Lavoie, E., Arola, D., and Wang, J. (2022). Microstructure, mechanical properties and elemental composition of the terrestrial isopod armadillidium vulgare cuticle. *J. Mech. Behav. BioMed. Mater* 132, 105299. doi: 10.1016/j.jmbbm.2022.105299

Yan, Z., Fang, Z., Ma, Z., Deng, J., Li, S., Xie, L., et al. (2007). Biomineralization: Functions of calmodulin-like protein in the shell formation of pearl oyster. *Biochim. Biophys. Acta* 1770, 1338–1344. doi: 10.1016/j.bbagen.2007.06.018

Yarra, T., Blaxter, M., and Clark, M. S. (2021). A bivalve biomineralization toolbox. *Mol. Biol. Evol.* 38, 4043–4055. doi: 10.1093/molbev/msab153

Yévenes, M., Núñez-Acuña, G., Gallardo-Escárate, C., and Gajardo, G. (2022). Adaptive mitochondrial genome functioning in ecologically different farm-impacted natural seedbeds of the endemic blue mussel *mytilus chilensis*. *Comp. Biochem. Physiol. Part D: Genomics Proteomics* 42, 100955. doi: 10.1016/j.cbd.2021.100955

Young, M. D., Wakefield, M. J., Smyth, G. K., and Oshlack, A. (2010). Gene ontology analysis for rna-seq: Accounting for selection bias. *Genome Biol.* 11, 1–12. doi: 10.1186/gb-2010-11-2-r14

Zhang, Y., Liu, Z., Song, X., Huang, S., Wang, L., and Song, L. (2019). The inhibition of ocean acidification on the formation of oyster calcified shell by regulating the expression of cgchs1 and cgchit4. *Front. Physiol.* 10, 1034. doi: 10.3389/fphys.2019.01034

Zieritz, A., Hoffman, J. I., Amos, W., and Aldridge, D. C. (2010). Phenotypic plasticity and genetic isolation-by-distance in the freshwater mussel *unio pictorum* (mollusca: Unionoida). *Evolutionary Ecol.* 24, 923–938. doi: 10.1007/s10682-009-9350-0